Cosmic Masers - from OH to H_0
Proceedings IAU Symposium No. 287, 2012
R.S. Booth, E.M.L. Humphreys & W.H.T. Vlemmings, eds.

doi:10.1017/S1743921312007326

Methanol Maser Parallaxes and Proper Motions

Y. Xu[1], M. J. Reid[2], L. Moscadelli[3], K. M. Menten[4], X. W. Zheng[5], A. Brunthaler[4], B. Zhang[4], K. L. J. Rygl[6], J. J. Li[1], and A. Sanna[4]

[1]Purple Mountain Observatory, China
email: xuye@pmo.ac.cn

[2]Harvard-Smithsonian Center for Astrophysics, USA

[3]Arcetri Obs., Italy

[4]Max-Planck-Institute für Radioastronomie, Germany

[5]Nanjing University, China

[6]INAF-IAPS, Italy

Abstract. Due to their compactness, persistence and slow motion, Class II CH_3OH masers are excellent targets for parallax and proper motion measurements for massive star-forming regions in the Galactic Disk. These measurements can be used to improve our understanding of the spiral structure and dynamics of the Milky Way. At the same time, Class II CH_3OH masers can also be used to study gas kinematics close to the exciting star, tracing rotation, infall and/or outflow motions.

Keywords. CH_3OH maser, parallaxes and proper motions, Galactic structure

1. Introduction

Class II CH_3OH masers at 6.7 and 12.2 GHz are strong (10-100 Jy), compact (typical spot size of a few milli-arcseconds (mas)), persistent (over many years), and are generally associated with slowly moving gas (velocities $\leqslant 10$ km s^{-1}). Thus, they are excellent astrometric targets. About a thousand 6.7 GHz and a hundred 12.2 GHz CH_3OH masers have been detected. Large numbers are located in the "molecular ring" and share the same spatial distribution as CO gas. Since the 6.7 and 12.2 GHz masers are always found in regions of on-going massive star-formation, they are good tracers of the spiral structure in the Galactic disk. In addition, they can also be used to infer the three-dimensional (3-D) gas kinematics around the massive (proto)stars at radii of tens to hundreds of astronomical unit (AU), which is not accessible via interferometric observations of thermal tracers.

2. Source of astrometric error

The spiral structure of the Milky Way is still poorly known. The classical model is mainly based on the kinematic distances (Georgelin & Georgelin 1976), which have been shown to be inaccurate (Xu *et al.* 2006) by up to 30% or more. Masers allow us a direct measurement of distances via trigonometric parallaxes; however, a (relative) positional accuracy of about 10 μas is necessary to determine accurate distances throughout the Milky Way. Achieving such an accuracy with Very Long Baseline Interferometry (VLBI) observations at centimeter wavelengths is not an easy task. Many factors can degrade the measurement accuracy. Systematic errors are related to the separation angle between target and calibrator, motivating one to find background calibrators close to the target.

Either the (maser) target or the background sources can be used as a phase-reference calibrator. If the maser target is strong enough to be detected within the interferometer coherence time, a quasar (QSO) as weak as a few mJy/beam can be revealed by imaging after applying the phase corrections derived from the maser. Statistically, the weaker the QSO, the higher the chance for it to be found near the maser. Using several interferometers (VLA, ATCA, MERLIN and VLBA), we have searched for weak QSOs and determined their positions accurately. Typically we find 3 suitable QSOs within 1 to 2 degrees of any CH_3OH maser source. Using multiple background calibrators helps in reducing systematic errors due to time variation in the atmosphere and in calibrator structure.

Poor knowledge of the vertical atmospheric delay for each station of the VLBI array is often the major source of systematic error in position. At high elevation angles, the VLBA correlator model is typically in error by about 10 cm of excess path length at 12 GHz, while at 6.7 GHz the model inaccuracy can be larger than 20 cm, dominated by ionospheric path delay. To achieve an astrometric accuracy $\leqslant$50 μas, it is crucial to remove the residual tropospheric and ionospheric effects, in particular for low-frequency observations. One way to measure and remove the tropospheric delays involves geodetic-like observing blocks. By observing about 15 QSOs, whose positions are known to better than 1 mas, the residual atmospheric delays above each antenna can be estimated accurately. Ionospheric (dispersive) delays can be partially removed by applying a global ionospheric model derived from GPS measurements. Our VLBA observations always include geodetic-like observing blocks and correct for the GPS ionospheric model during the data calibration.

One other source of observational error comes from the absolute position of the phase-reference calibrator. If the error in the correlated position of the calibrator is $\geqslant$10 mas, the phase-referenced image can be distorted and affected by second-order positional errors. To be able to detect weak (a few mJy/beam) signals in the phase-reference map, it is therefore important to know the calibrator position with high accuracy. Note that most of the VLBA calibrators have a position accuracy of $\sim$1 mas.

3. Parallaxes and proper motions

After calibrating and removing the sources of error discussed in the previous section, one can measure parallaxes and proper motions of the CH_3OH masers with high accuracy. Figure 1 shows the results for the 12 GHz masers towards the UC HII region W3(OH). It displays the sky-projected trajectory of a single 12 GHz CH_3OH maser spot relative to three QSOs, which results from the sum of the annual parallax, Solar Motion, differential Galactic rotation, peculiar motion (of the target star with respect to *its* Local standard of rest (LSR)) and internal motion (of the maser spot with respect to the star. The projection of the maser spot path on each equatorial coordinate (RA and Dec) can be fitted with a linear plus a sinusoidal motion, the latter reflecting the annual parallax. For W3(OH), we obtain a parallax of 512$\pm$10 μas and spot proper motions are derived with an accuracy of $\sim$1 km s^{-1}(Xu *et al.* 2006). Such a parallax accuracy is enough to measure distances to $\sim$ 10 kpc, comparable with the size of the Milky Way disk, with 10% uncertainty.

In the last years, the 6.7 GHz methanol masers were successfully used for parallax measurements with the European VLBI Network, achieving accuracies approaching 20 μas (Rygl *et al.* 2010). The obtained distances were found to be in agreement with VERA water masers parallaxes (Sato *et al.* 2008, Nagayama *et al.* 2011) for two star-forming regions. Recently, the distance to the Cygnus X region was measured using 6.7

https://doi.org/10.1017/S1743921312007326 Published online by Cambridge University Press

GHz methanol masers. The parallaxes toward four star-forming regions, W 75N, DR 21, DR 20, and IRAS 20290+4052 in Cygnus X North, were found to be consistent with a single distance of 1.40 ± 0.08 kpc for the Cygnus X complex (Rygl *et al.* 2012). Figure 2 shows the parallax fit of W 75N based on 10 masers spots observed in eight EVN epochs. The resulting parallax was 0.772 ± 0.042 mas, which corresponds to a distance of 1.30 ± 0.07 kpc.

To date, the CH_3OH masers have been used to determine, parallaxes and proper motions for 26 massive star-forming regions (Bartkiewicz *et al.* 2008, Reid *et al.* 2009a, Moscadelli *et al.* 2009, Xu *et al.* 2009, Xu *et al.* 2011, Zhang *et al.* 2009, Brunthaler *et al.* 2009, Sanna *et al.* 2009, Rygl *et al.* 2010, Rygl *et al.* 2012), tabulated in Table 1. Most of them have parallax accuracy of better than 10%. Reid *et al.* (2009b) modeled 18 parallaxes available in 2009 and found that massive star-forming regions lag circular rotation by about 15 km s^{-1}. This provided motivation for a re-analysis of the Solar Motion by Schönrich *et al.* (2010), resulting in an increase in the component in the direction of Galactic rotation by 7 km s^{-1}, and a corresponding reduction in the star forming region velocity lag.

We can update these model results based on the 26 parallax/proper motions. In the frame rotating with the Galaxy, taking the distance to the Galactic center of 8.3 kpc and circular rotation speed of 239 km s^{-1} Brunthaler *et al.* (2011), and the updated Solar Motion values from Schönrich *et al.* (2010), we find an average lag of 12 km s^{-1}in the direction of Galactic rotation and an average motion of 11 km s^{-1} toward Galactic cen-

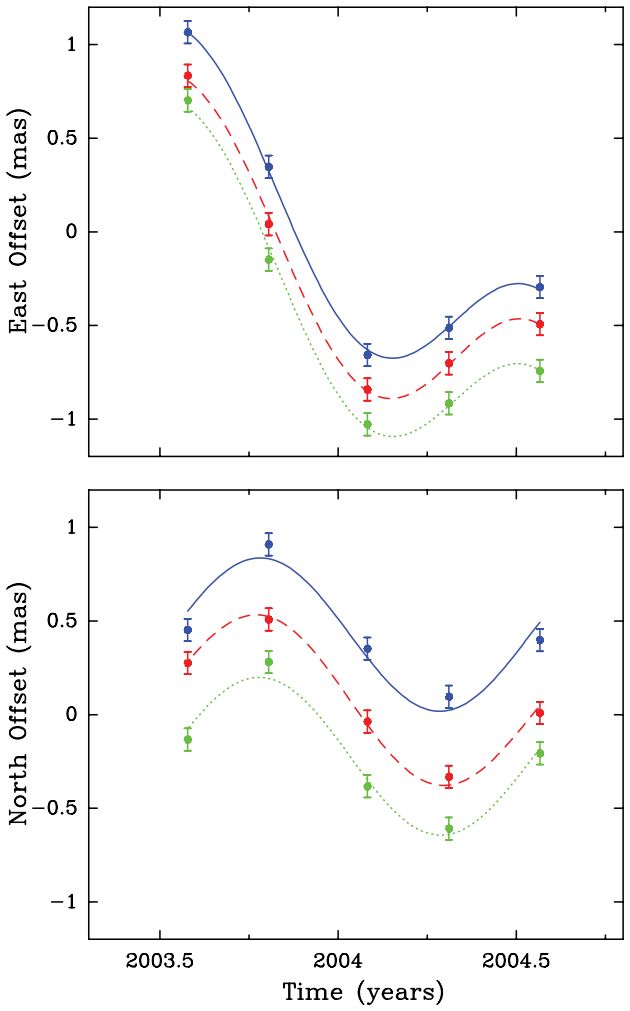

Figure 1. Position versus time for a maser spot relative to each QSO in W3OH.

https://doi.org/10.1017/S1743921312007326 Published online by Cambridge University Press

ter (see Figure 3) However, one can see that G9.62+0.20 & G23.6-0.1 have large peculiar motions, probably caused by the gravitational potential of the bar making them unsuitable for studying average systematic motions. If we drop them and use the remaining 24 sources we find, similar to Reid *et al.* (2009b), on average a systematic motion of 5 km s^{-1} toward the Galactic center and 7 km s^{-1} of counter rotation. Since the CH_3OH masers are only associated with massive star-forming regions, this indicates that newly formed massive stars orbit the Milky Way ∼7 km s^{-1} slower than for circular orbits and ∼5 km s^{-1} towards the Galactic center. The systematic motions might be caused by a wrong estimate of the Solar Motion and an inadequate Galaxy rotation curve, while the accurate values would be obtained by the BeSSeL project.

4. Gas kinematics close to the massive (proto)star

Presently massive star-formation is a very active field of research but several theoretical issues associated with the ionization action and the dynamical effects of the radiation from the massive (proto)star on the surrounding gas are still unclear. However, the observation of massive star-forming regions is severely limited by the large distances (typically of several kpc) and the clustered formation mode, which prevent detailed studies of single (proto)stellar-systems, with all but VLBI observations of their associated maser emission.

For several years, we have been conducting a campaign of multi-epoch VLBI observations of the strongest interstellar molecular masers (OH at 1.6 GHz, CH_3OH at 6.7 GHz, and H_2O at 22 GHz) towards a small sample of massive star-forming regions (Moscadelli *et al.* 2007, 2011; Sanna *et al.* 2010; Goddi *et al.* 2011). One of the major results of our observations is the result that the (VLBI measurable) 3-D velocity distribution of

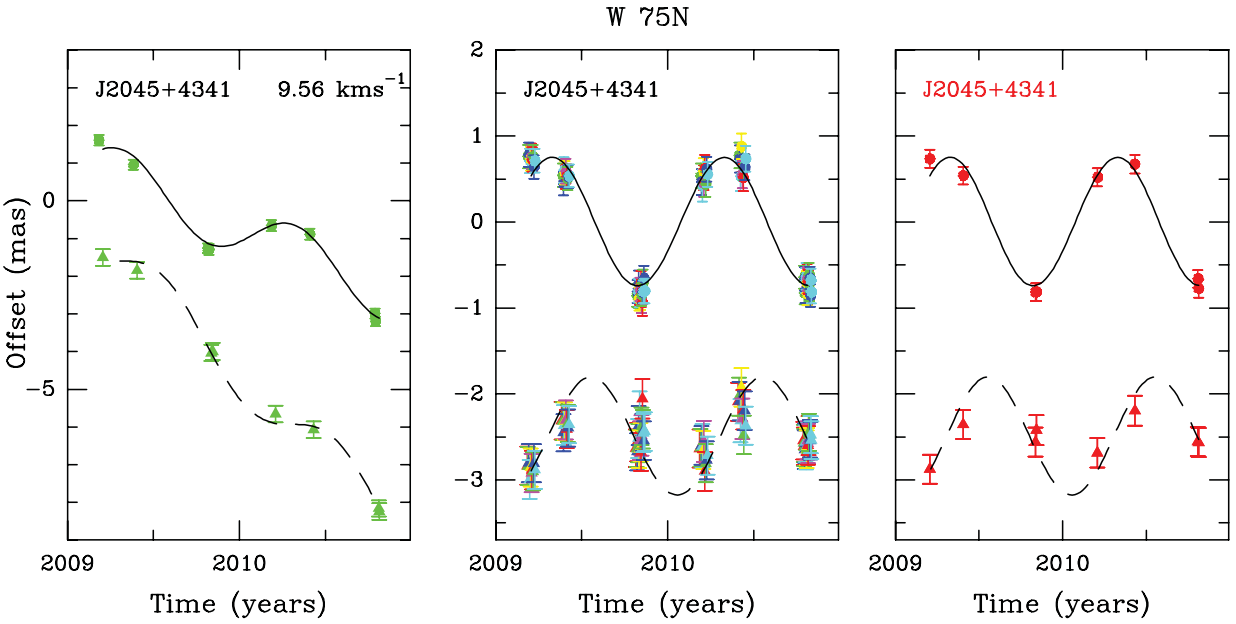

Figure 2. Results of the parallax fit for W 75N using QSO J2045+4341 as position reference. *Left panel:* Results of the parallax fit for the maser spot at $V_{\rm LSR}$ = 9.56 km s^{-1} without the removal of the proper motions. The right ascension and declination data have been offset for clarity. *Middle and right panel:* Results of the parallax fit for W 75N after removing proper motions and positional offsets; combined fit on 10 maser spots (*middle panel*) and fit to the averaged data of the 10 maser spots (*right panel*). The declination data have been offset for clarity. The dots mark the data points in right ascension, while the filled triangles mark the declination data points. The solid lines show the resulting parallax fit in right ascension and the dashed lines show the fit in declination. The scale of the Y-axis of the *middle* and *right panels* is different from the scale of the *left panel*.

https://doi.org/10.1017/S1743921312007326 Published online by Cambridge University Press

Table 1. Parallaxes and Proper Motions of High-mass Star-Forming Regions.

Source	l (deg)	b (deg)	Parallax (mas)	μ_x (mas yr^{-1})	μ_y (mas yr^{-1})	v_{LSR} (km s^{-1})	Maser (GHz)
G9.62+0.20	9.62	+0.20	0.194 ± 0.023	−0.580± 0.054	−2.49 ± 0.27	+2 ± 5	12
G12.89+0.49	12.89	+0.49	0.452 ± 0.029	+0.20 ± 0.04	−1.74 ± 0.76	+34 ± 3	12
G15.03−0.68	15.03	−0.68	0.505 ± 0.033	+0.68 ± 0.05	−1.42 ± 0.09	+20 ± 3	12
G 23.0−0.4	23.01	−0.41	0.218 ± 0.017	−1.72 ± 0.04	−4.12 ± 0.30	+81 ± 3	12
G 23.4−0.2	23.44	−0.18	0.170 ± 0.032	−1.93 ± 0.10	−4.11 ± 0.07	+97 ± 3	12
G 23.6−0.1	23.66	−0.13	0.313 ± 0.039	−1.32 ± 0.02	−2.96 ± 0.03	+83 ± 3	12
G27.36−0.16	27.36	−0.16	0.125 ± 0.042	−1.81 ± 0.08	−4.11 ± 0.26	+92 ± 3	12
G 35.2−0.7	35.20	−0.74	0.456 ± 0.045	−0.18 ± 0.06	−3.63 ± 0.11	+28 ± 3	12
G 35.2−1.7	35.20	−1.74	0.306 ± 0.045	−0.71 ± 0.05	−3.61 ± 0.17	+42 ± 3	12
W 51 IRS 2	49.49	−0.37	0.195 ± 0.071	−2.49 ± 0.08	−5.51 ± 0.11	+56 ± 3	12
G 59.7+0.1	59.78	+0.06	0.463 ± 0.020	−1.65 ± 0.03	−5.12 ± 0.08	+27 ± 3	12
ON 1	69.54	−0.98	0.389 ± 0.045	−3.24 ± 0.89	−5.42 ± 0.46	+12 ± 1	6.7
IRAS 20126+4104	78.12	+3.63	0.61 ± 0.02	−4.14 ± 0.13	−4.14 ± 0.13	−3.5± 3	6.7
IRAS 20290+4052	79.74	+0.99	0.737 ± 0.062	−2.84 ± 0.09	−4.14 ± 0.54	−1.4±3	6.7
DR 20	80.86	+0.38	0.687 ± 0.038	−3.29 ± 0.13	−4.83 ± 0.26	−3.0±3	6.7
DR 21	81.74	+0.59	0.666 ± 0.035	−2.84 ± 0.15	−3.80 ± 0.22	−3.0±3	6.7
W 75N	81.87	+0.78	0.772 ± 0.042	−1.97 ± 0.10	−4.16 ± 0.15	+9.0± 3	6.7
L 1206	108.18	+5.52	1.289 ± 0.153	+0.27 ± 0.23	−1.40 ± 1.95	−10 ± 3	6.7
Cep A	109.87	+2.11	1.430 ± 0.080	+0.50 ± 1.10	−3.70 ± 0.20	−10 ± 5	12
NGC 7538	111.54	+0.78	0.378 ± 0.017	−2.45 ± 0.03	−2.44 ± 0.06	−57 ± 3	12
L 1287	121.30	+0.66	1.077 ± 0.039	−0.86 ± 0.11	−2.29 ± 0.56	−18 ± 3	6.7
NGC 281-W	123.07	−6.31	0.421 ± 0.022	−2.69 ± 0.16	−1.77 ± 0.11	−32 ± 3	6.7
W3(OH)	133.95	+1.06	0.512 ± 0.010	−1.20 ± 0.20	−0.15 ± 0.20	−45 ± 3	12
S 252	188.95	+0.89	0.476 ± 0.006	+0.02 ± 0.01	−2.02 ± 0.04	+11 ± 3	12
S 255	192.60	−0.05	0.628 ± 0.027	−0.14 ± 0.54	−0.84 ± 1.76	+8 ± 3	6.7
G 232.6+1.0	232.62	+1.00	0.596 ± 0.035	−2.17 ± 0.06	+2.09 ± 0.46	+23 ± 3	12

water masers, emerging from shocked molecular gas at the interface between the fast flowing and the ambient material, efficiently trace the structure of (proto)stellar outflows close to (within 10–100 AU) the (proto)star. Our study also provides evidence that the methanol masers are found at (relatively) large separations from the protostellar jet

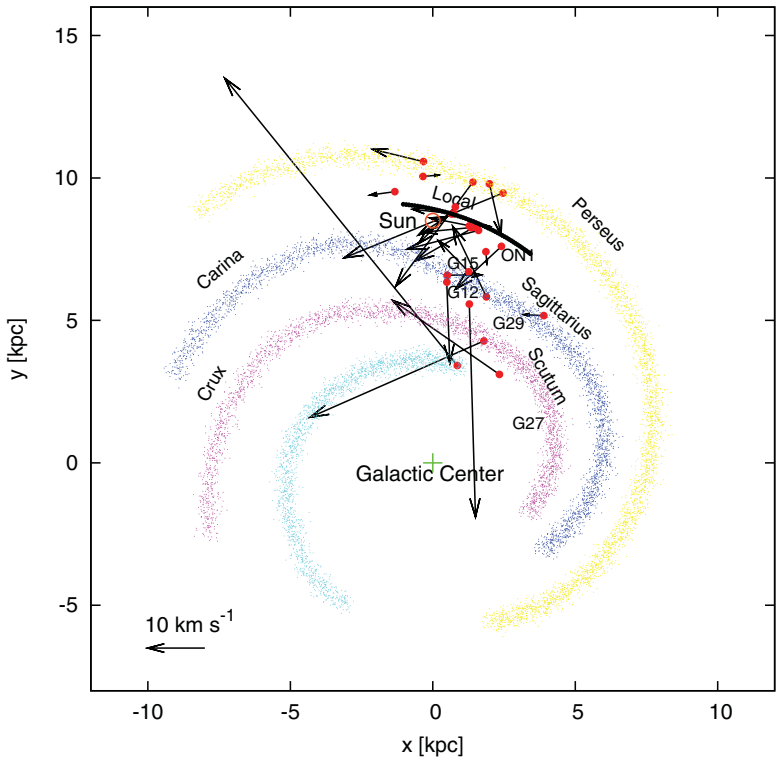

Figure 3. Peculiar motions of massive star forming regions. The amplitude scale is given at the bottom.

https://doi.org/10.1017/S1743921312007326 Published online by Cambridge University Press

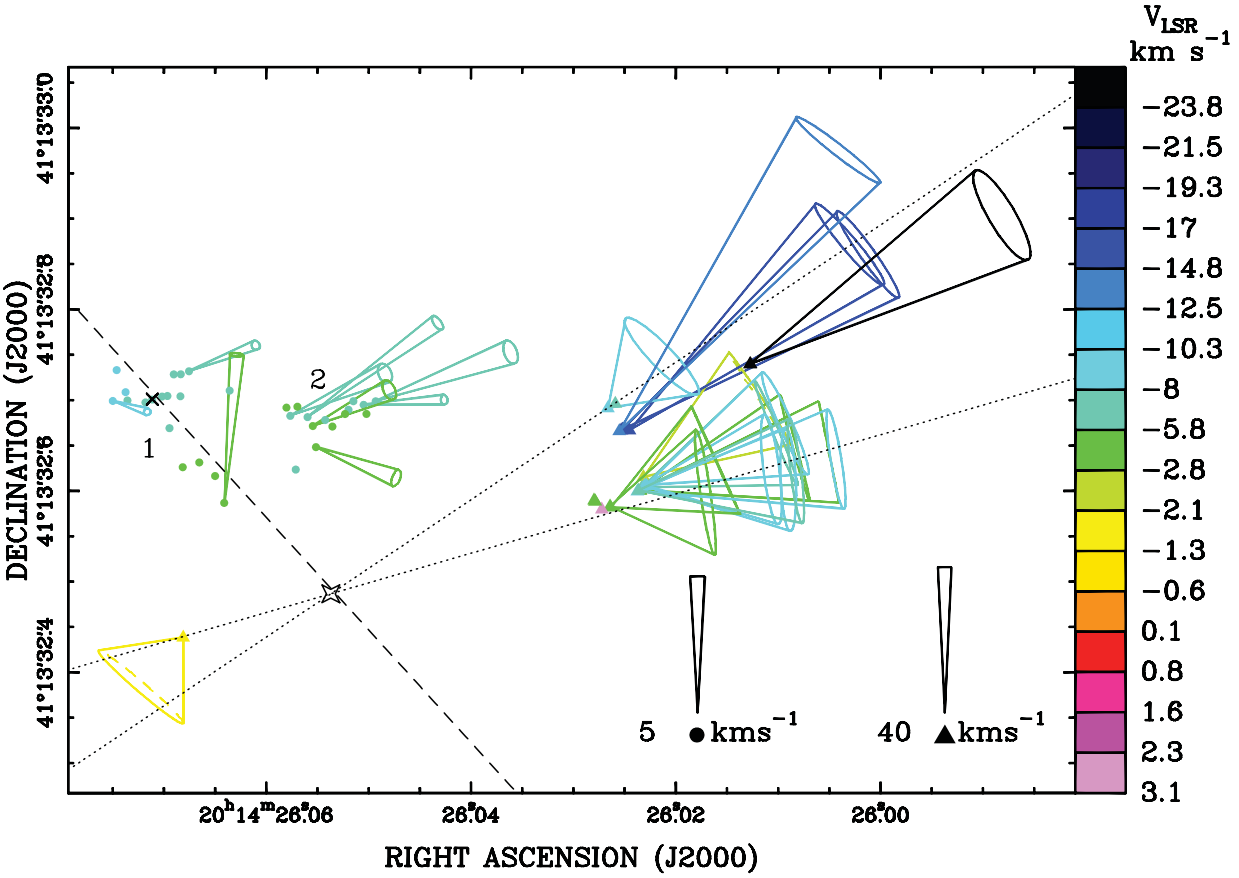

Figure 4. Water (triangles) and 6.7 GHz methanol (circles) masers in IRAS 20126+4104. The cones indicate the 3D velocities of the maser features with respect to the star, for the H_2O masers, or relative to a chosen feature (marked with a cross), for the CH_3OH masers. Points without an associated cone have been detected only at one or two epochs and the associated proper motion cannot be computed or is considered unreliable. The cone opening angle corresponds to 1σ motion uncertainties. The length of the cones is proportional to the speed, with different scales used for the two maser types as indicated in the figure. The colours correspond to the line of sight velocities, as shown in the colour scale to the right. The starred polygon marks the location of the star, obtained from the model fit to the H_2O maser positions and 3D velocities. Labels "1" and "2" denote two elongated groups of CH_3OH maser features. The dotted line outline the projection of the bipolar H_2O maser jet onto the plane of the sky, while the dashed line is a linear fit to the CH_3OH maser features of group 1.

and trace more quiescient gas than the water masers. In the following we describe the results obtained towards the sources IRAS 20126+4104 and AFGL5142. In the former, the 6.7 GHz CH_3OH masers might originate a the Keplerian disk, partly rotating with the disk material and partly being entrained into a slow disk-wind. In the latter, we found evidence that the CH_3OH masers emerge from an infalling envelope at a radius of ≈300 AU from the protostar.

4.1. *IRAS 20126+4104*

Figure 4 shows positions and velocities of the 22 GHz H_2O and 6.7 GHz CH_3OH masers towards the intermediate-massive protostar IRAS 20126+4104. The H_2O maser velocities trace a bipolar, collimated, NE–SW oriented outflow at a distance of a few hundred AU from the star. Moscadelli *et al.*(2011), by fitting a simple model of a conical jet, derive the main parameters of the water maser outflow: an outflow axis PA of 115°, an inclination with respect to the line-of-sight (LOS) of 80°, an opening angle of 18°, and the position of the central star (i.e., the cone vertex) with an accuracy of ≈100 mas.

The 6.7 GHz methanol masers are clustered to the NE of the star and their positions

https://doi.org/10.1017/S1743921312007326 Published online by Cambridge University Press

and LOS velocities are compatible with their origin from the northeastern side of the Keplerian disk detected in several high-density thermal tracers about the star (Cesaroni *et al.* 1997). Looking at Fig. 4, one sees that the CH_3OH maser features are roughly outlining two linear structures, one oriented NE–SW (group 1) and the other SE–NW (group 2). Moscadelli *et al.* (2011) have calculated the *relative* proper motions (see Fig. 4) of the CH_3OH maser features of both groups with respect to a feature belonging to group 1, which appears to be the most reliable for the persistency of the internal structure over the observing epochs.

It is worth noting two facts. First, the masers in group 2 move towards NW, i.e. in the same direction as the blue lobe of the H_2O maser jet. Despite the different speeds (up to ∼100 km $s^{-1}$for H_2O and only ∼5 km s^{-1} for CH_3OH), this suggests a relationship between the two. Second, the mean velocity of group 1 features along the line of sight is –6.9 km s^{-1}, which differs by –3.4 km s^{-1} with respect to the systemic LSR velocity of –3.5 km s^{-1}. The mean distance of the same features from the nominal position of the star (starred symbol in Fig. 4) is 0.″27 or ∼460 AU. If the masers are undergoing Keplerian rotation about the 7 $M_\odot$ star, the expected velocity is ~ -3.7 km s^{-1}, consistent with the value of –3.4 km s^{-1} quoted above.

Based on this, Moscadelli *et al.* (2011) proposed that group 1 masers trace the Keplerian disk, while for group 2 masers it is suggested that they also lie in the disk, but very close to the transition region between the disk surface and the outer part of the jet. This hypothesis may explain why the relative proper motions of group 2 features (see Fig. 4) are roughly perpendicular to the plane of the disk. Group 2 features could be tracing material lifted from the disk surface and accelerated along the rotation axis. This scenario is reminiscent of the MHD "disk wind", driven by the toroidal magnetic pressure (see, e.g., Banerejee & Pudritz 2005 and references therein), invoked to explain the formation of large scale outflows in Young Stellar Objects.

4.2. *AFGL5142*

Figure 5 shows the proper motions of the 22 GHz water masers (left panel) and 6.7 GHz methanol masers (right panel) measured towards the millimeter core AFGL 5142 MM-1 by Goddi *et al.* (2011). The high-angular resolution maps show a collimated bipolar outflow, at radii 140 to 400 AU, traced by radio continuum emission from its ionized component and by water masers from its molecular component. The two peaks of radio continuum emission are associated with the two clusters of water masers which are expanding, suggesting that the radio continuum probably comes from an ionized jet.

Looking at the right panel of Figure 5, the 6.7 GHz CH_3OH yellow spots have relatively large proper motions, directed towards the geometric center of the red features, which move mostly along the LOS, indicating motions towards the protostar. Since all methanol masers are seen in the foreground of the 22 GHz continuum emission (which is optically thick at 6.7 GHz) and have red-shifted LOS velocities, they most likely trace infall toward the protostar. Goddi *et al.* (2011) have reproduced the methanol maser velocity distribution with a simple model of spherical infall, deriving a central mass of 4 ± 1 $M_\odot$, a radius for the infalling envelope of 290 ± 70 AU, an infall velocity of 5 ± 1 km s^{-1}, and a stellar position (i.e., the sphere center) coincident (within the fit error of 20 mas) with the geometric center of the red features. The derived mass infall rate of 6×10^{-4} $M_\odot$ yr^{-1} implies a protostellar age $\lesssim 10^{-4}$ yr. Note that methanol masers, for the first time, show evidence of infall of material on to the protostar from the 3-D velocity field of molecular gas.

https://doi.org/10.1017/S1743921312007326 Published online by Cambridge University Press

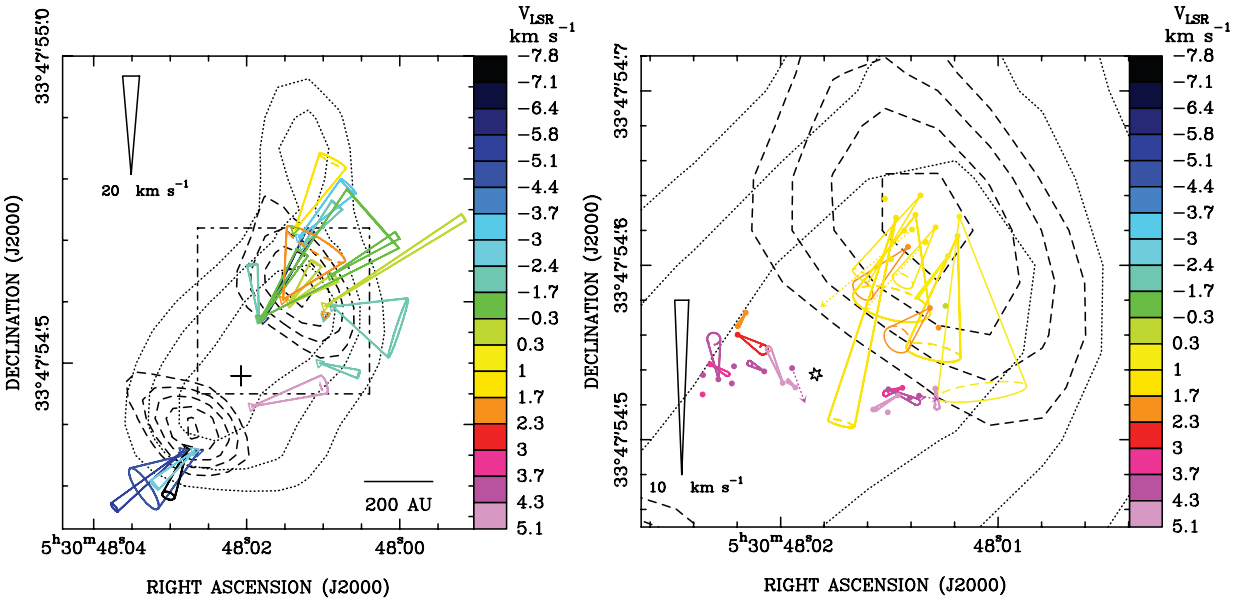

Figure 5. Proper motions of H_2O (*Left panel*) and CH_3OH (*Right panel*) masers measured towards AFGL 5142 MM-1. The dot-dashed rectangle in the left panel shows the area plotted in the right panel. The colored cones indicate proper motion orientation and uncertainties for individual maser features (the amplitude scale is given at the left of each panel). Colors denote line-of-sight velocities and contour maps show the 22 GHz (dotted line) and 8.4 GHz (dashed line) continuum emissions observed with the VLA. The black star in the right panel identifies the expected location of the protostar, corresponding to the geometric mean of positions of the red methanol masers. Water masers and radio continuum together identify a collimated bipolar (ionized/molecular) outflow.

5. Summary

1. Class II CH_3OH masers are closely associated with massive star formation and are very good targets for astrometry because they are compact, long lived and slow moving.
2. Parallax accuracies of better than 10 μms have been obtained for CH_3OH masers, indicating that they can be used to construct the spiral structure throughout the Milky Way's disk.
3. They can be used to study the Solar Motion and the Galaxy's rotation curve.
4. They can also be used to study the gas kinematics close to the exciting star, which might trace rotation, infall and/or outflowing motion.

Acknowledgements

This work was supported by the Chinese NSF through grants NSF 11133008, NSF 11073054, NSF 10621303, NSF 10733030 and the Key Laboratory for Radio Astronomy, CAS. K.L.J.R is funded by an ASI fellowship under contract number I/005/07/1.

References

Banerjee, R. & Pudritz, R. E. 2005, "Outflows and Jets from Collapsing Magnetized Cloud Cores", Protostars and Planets V, 2005.

Bartkiewicz, A., Brunthaler, A., Szymczak, M. van Langevelde, H. J & Reid, M. J. 2008, *A&A*, 490, 787

Brunthaler, A., Reid, M. J, Menten, K. M. *et al.* 2011, *AN*, 332, 461

Brunthaler, A., Reid, M. J., Menten, K. M., Zheng, X. W., Moscadelli, L., & Xu, Y. 2009, *ApJ*, 693, 424

Cesaroni, R., Felli, M., Testi, L., Walmsley, C. M., & Olmi, L. 1997, *A&A*, 325, 725

https://doi.org/10.1017/S1743921312007326 Published online by Cambridge University Press

Dehnen, W. & Binney, J. J., *MNRAS*, 1998, 298,387
Georgelin, Y. M. & Georgelin, Y. P., 1976, *A&A*, 49, 57
Goddi, C., Moscadelli, L., & Sanna, A. 2011, *A&A*, 535, L8.
Moscadelli, L., Reid, M. J., Menten, K. M., Brunthaler, A., Zheng, X. W., & Xu, Y. 2009, *ApJ*, 693, 406
Moscadelli, L., Cesaroni, R., Rioja, M. J., Dodson, R., & Reid, M. J. 2011, *A&A*, 526, 66
Nagayama, T., Omodaka, T., Nakagawa, A., *et al.* 2011, *PASJ*, 63, 23
Reid, M. J., Menten, K. M., Brunthaler, A., Zheng, X. W., Moscadelli, L., & Xu, Y. 2009, *ApJ*, 693, 397
Reid, M. J., Menten, K. M., Zheng, X. W. *et al.* 2009, *ApJ*, 700, 137
Rygl, K. L. J., Brunthaler, A., Reid, M. J., Menten, K. M., van Langevelde, H. J., & Xu, Y. 2010, *A&A*, 511, 2
Rygl, K. L. J., Brunthaler, A., Sanna, A. *et al.* 2012, *A&A*, 539, 79
Sanna, A., Reid, M. J., Moscadelli, L., Dame, T. M., Menten, K. M., Brunthaler, A., Zheng, X. W., & Xu, Y. 2009, *ApJ*, 706, 464
Sanna, A., Moscadelli, L., Cesaroni, R., Tarchi, A., Furuya, R. S., & Goddi, C. 2010, *A&A*, 517, A78
Sato, M., Hirota, T., Honma, M., *et al.* 2008, *PASJ*, 60, 975
Schönrich, R., Binney, J. J., & Dehnen, W., 2010, *MNRAS*, 403, 1829
Xu, Y., Reid, M. J., Zheng, W. W., & Menten, K. M. 2006, *Science*, 311, 54
Xu, Y., Reid, M. J., Menten, K. M., Brunthaler, A., Zheng, X. W., & Moscadelli, L. 2009, *ApJ*, 693, 413
Xu, Y., Moscadelli, L., Reid, M. J. *et al.*, 2011, *ApJ*, 733, 25
Zhang, B., Zheng, X. W., Reid, M. J., Menten, K. M., Xu, Y., Moscadelli, L., & Brunthaler, A. 2009, *ApJ*, 693, 419

https://doi.org/10.1017/S1743921312007326 Published online by Cambridge University Press